Journal of Power Sources 196 (2011) 6517–6524

Contents lists available at ScienceDirect

Journal of Power Sources

journal homepage: www.elsevier.com/locate/jpowsour

Thermal analysis and management of lithium–titanate batteries

Michael R. Giuliano, Suresh G. Advani, Ajay K. Prasad *

Center for Fuel Cell Research, Department of Mechanical Engineering, University of Delaware, Newark, DE 19716, United States

ARTICLE INFO

Article history:
Received 27 February 2011
Received in revised form 30 March 2011
Accepted 31 March 2011
Available online 8 April 2011

Keywords:
Battery electric vehicle
Hybrid electric vehicle
Lithium–titanate battery
Thermochromic liquid crystals
Thermal analysis
Battery cooling

ABSTRACT

Battery electric vehicles and hybrid electric vehicles demand batteries that can store large amounts of energy in addition to accommodating large charge and discharge currents without compromising battery life. Lithium–titanate batteries have recently become an attractive option for this application. High current thresholds allow these cells to be charged quickly as well as supply the power needed to drive such vehicles. These large currents generate substantial amounts of waste heat due to loss mechanisms arising from the cell's internal chemistry and ohmic resistance. During normal vehicle operation, an active cooling system must be implemented to maintain a safe cell temperature and improve battery performance and life. This paper outlines a method to conduct thermal analysis of lithium–titanate cells under laboratory conditions. Thermochromic liquid crystals were implemented to instantaneously measure the entire surface temperature field of the cell. The resulting temperature measurements were used to evaluate the effectiveness of an active cooling system developed and tested in our laboratory for the thermal management of lithium–titanate cells.

1. Introduction

The growing popularity of battery electric vehicles (BEV) and hybrid electric vehicles (HEV) has created a demand for efficient, lightweight, durable, and safe batteries. Lithium-ion batteries are preferred for EVs as they offer high energy density and good cycle life. In addition, they are generally safe and do not suffer from memory effects. In EV applications, these batteries need to accommodate high currents over many charge and discharge cycles. In order to achieve the voltage necessary to power an EV, many cells must be connected in series to create a battery pack that will likely be confined to an internal compartment within the vehicle. When in use, each cell will generate heat throughout its volume due to loss mechanisms arising from the cell's internal chemistry and ohmic resistance. The battery's large current demand, and the proximity of individual cells to one another within the battery pack which is itself situated in a confined region, make thermal management a high priority concern for the proper functioning and safety of EVs.

Recent advances in Li-ion technology have led to the development of lithium–titanate batteries which, according to one manufacturer, offer higher energy density, more than 2000 cycles (at 100% depth-of-discharge), and a life expectancy of 10–15 years [1]. The objective of this work is to characterize the temperature rise due to heat generation during charge and discharge in a lithium–titanate battery and explore methods for thermal management. A technique based on thermochromic liquid crystals was devised to instantaneously measure the temperature field over the entire surface of the battery. This measurement technique was used to analyze and evaluate an active cooling system designed to maintain an internal cell temperature of less than 50 °C which is below the maximum operating temperature of 55 °C as specified by the manufacturer. Additionally, the energy balance equation was applied to the coolant flow at steady state to estimate the total heat generated by each cell under different current demands.

The cells tested in this work are manufactured by Altairnano and have a maximum voltage of 2.79 V, a 50 Ah capacity, and can accommodate currents up to 400 A. They have also been shown to handle a large number of charge/discharge cycles. However, without an active cooling system, the cell temperature within the battery pack can potentially exceed the maximum operating temperature of 55 °C during normal operation. Hence, implementing an effective cooling system is an essential requirement for this type of battery. According to the manufacturer, thermal runaway is not a concern with these cells below 250 °C due to the use of nanostructured electrode materials [1]. Additional benefits from good thermal management of lithium–titanate cells include improved electrochemical performance, better charge acceptance, higher power and energy capacity, and improved cycle life.

Preliminary tests revealed that the cells do not generate heat evenly throughout their volume. It can be easily understood that the current flux within the cell increases steadily from the edges of the cell to its terminal, implying a greater heat generation as the terminal is approached. For this reason, a system for measuring the temperature of the cell over its entire surface had to be devised.

* Corresponding author. Tel.: +1 302 831 2960; fax: +1 302 831 3619.
E-mail address: prasad@udel.edu (A.K. Prasad).

0378-7753/$ – see front matter © 2011 Elsevier B.V. All rights reserved.
doi:10.1016/j.jpowsour.2011.03.099

In many cases an infrared camera is used for this type of surface measurement [2]. This solution, however, could not be used in our application due to the particular construction of the cell. Each cell has a loose-fitting aluminum jacket around it that does not make complete contact with the cell itself. Acquiring an infrared image of the cell without pressing the jacket against the cell's interior will not yield an accurate surface temperature measurement due to inadequate thermal contact between the cell and its jacket. In order to ensure proper thermal contact while also allowing visual access to the front of the cell, the cell would have to be compressed between transparent plastic or glass panels. Unfortunately, such materials act as infrared blockers and hence would contaminate the infrared signal from the surface of the cell. While infrared technology is extremely useful in some circumstances, our unique needs precluded its use in our study.

Another option for measurement of surface temperatures is discussed in [3]. This method involves fixing thermocouples to the surface of the cell at different locations. This method also presents problems in our application. The first issue is physically adhering the thermocouples to the cell. We require the complete insulation of the front and back face of the batteries. Placing multiple thermocouples on one of these faces would create a small air gap between the cell and the insulation layer thereby reducing the effectiveness of our insulation. More importantly, thermocouples are point wise measurement devices and would restrict our ability to determine the entire surface temperature distribution of the cell. While thermocouples provide very accurate temperature measurements, our application would require a large array of thermocouples further complicating the insulation process.

To bypass these issues, we employed thermochromic liquid crystal (TLC) thermography. TLCs are organic molecules that change color with temperature. They are characterized by two temperatures: Red Start, which is the temperature at which color play commences, and Bandwidth which is the temperature range over which the TLC transits the color spectrum from red (cold) to blue (hot). TLCs can be ordered with customized red starts and bandwidths. They are available as adhesive-backed sheets from Hallcrest, and can be applied to the desired surface very easily. Since the TLC strips are very thin, they respond rapidly to temperature changes of the substrate. In order for TLCs to provide accurate quantitative temperature information over extended two-dimensional domains, they must be properly calibrated to create a mapping between color and temperature. Temperature visualization with TLCs has been practiced for many years, and several papers can be found in the literature describing the most effective way to perform liquid crystal thermography [4–6]. Following the procedures outlined in these papers the TLC layer can be used to determine surface temperature for time-varying applications. TLC technology coupled with thermistors can provide the entire temperature field of the cell without compromising the cell's insulation. Therefore, TLC thermography provides an effective method to evaluate the thermal performance of the battery system under various operating conditions, and to evaluate the effectiveness of battery cooling systems.

Ultimately, this work can assist in the development of a battery thermal model for this type of cell. Although thermal models of batteries have been developed for many different geometries and cell properties [7–12], experimental studies of the thermal characteristics of batteries are scarce. The goal of this paper is to experimentally acquire thermal data of lithium–titanate cells under realistic conditions in order to construct an accurate thermal model in the future. For example, given the entire time-varying temperature field of the cell during charge–discharge cycling, an iterative method can be implemented to extract the heat generation source term that varies throughout the volume of the cell. This source term is necessary to construct an accurate finite element model of the cell. The model can then be used to design and evaluate a multitude of thermal management systems in software prior to actual construction.

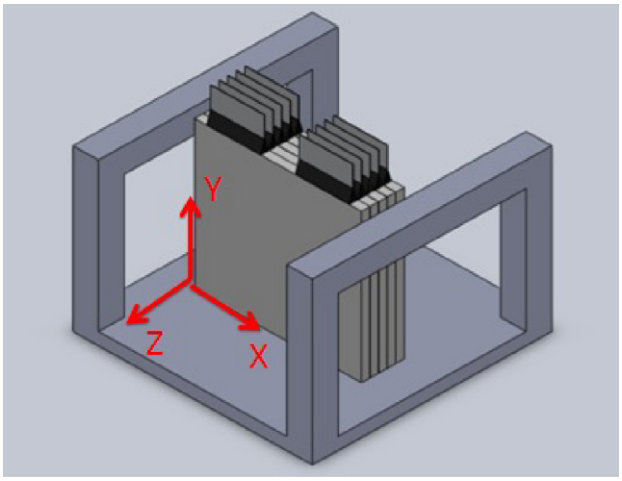

Fig. 1. Solid model of the test stand for battery experiments.

The following sections will describe the procedure used to calibrate the TLCs, the protocols used to conduct temperature measurements of the cells under various charge and discharge currents, and a demonstration of the effectiveness of a selected cooling system. Conclusions will also be drawn about the nature of heat generation including results that will aid in the design of future cooling systems.

2. Experimental procedure

2.1. Test stand

To simulate batteries in the center bank on an EV, a test stand was developed to house a stack of five cells insulated on the front and the back. A solid model of the 5-cell stack is shown in Fig. 1 in a simplified version of the test stand. Each cell is 247 mm × 228 mm, and is 13 mm thick. The cell has two rectangular tabs (38 mm × 76 mm) that serve as its terminals.

In order to understand the thermal behavior of the stack, we focused on the cell in the front of the stack. Fig. 2 is a detailed solid model of the first cell. Five TLC strips (each 228 mm long and 11 mm wide) were attached to the surface of the cell symmetrically about its vertical axis as shown. The strips were arranged such that temperature range of each strip increases in 5-degree increments from left to right. Five separate temperature ranges were chosen to obtain a more vivid color play and improve the resolution and accuracy of our temperature measurements. This arrangement allowed us to monitor the surface temperature of the cell within the combined bandwidth of 25–50 °C. In order to replicate the actual conditions within the battery pack on an EV, the front and back faces of the stack were insulated. In particular, the front of the cell was insulated by employing a double-paned, plexiglass window because it permitted visual access of the TLC. Temperature visualization with TLC provided valuable insights into the nature of heat generation in these cells.

The positive and negative terminals are marked on the top of the cell in Fig. 2. When the cells are connected to one another in series, the tabs from one cell are clamped to those of the adjacent cells. This type of connection is not ideal and results in heat generation at each junction due to contact resistance:

$$q = I^2R \quad (1)$$

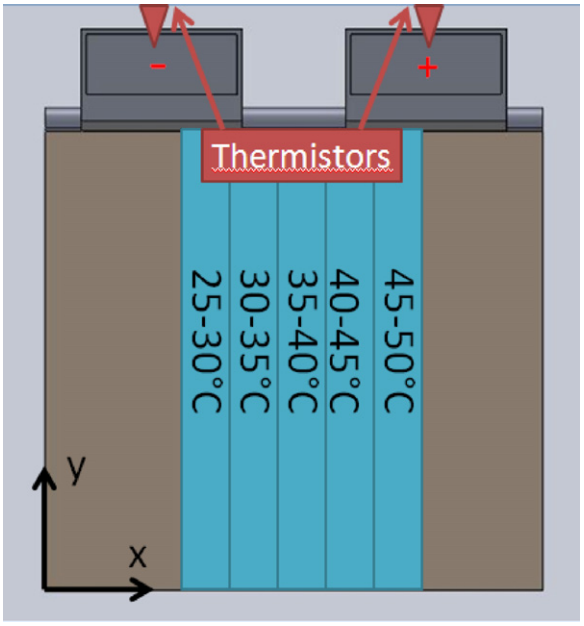

Fig. 2. Schematic view of the front cell of the stack. Five TLC strips with temperature ranges in 5° increments were attached to the surface of the cell as shown. Thermistor locations on the tabs are also indicated.

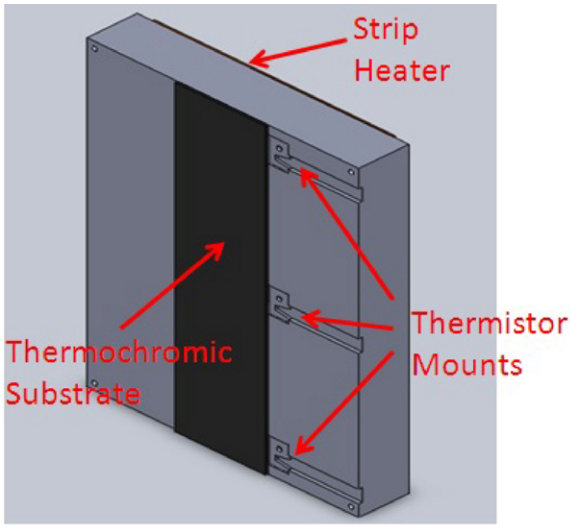

Fig. 3. Heater block used for TLC calibration. The block is 50 mm thick and made out of aluminum to allow for even heat distribution, and includes three slots for thermistors.

where q is the heat generated, I is the current, and R is the contact resistance. Heat is also generated within the body of the cell due to its internal resistance to current flow, and due to the electrochemical reactions that occur during charge and discharge. The current densities are much higher in the upper region of the cell because all of the current generated across the face of the cell during discharge has to converge at the terminals where it is collected. Similarly, during charging, all of the current supplied to the cell travels through the tabs before it gets distributed throughout the entire volume of the battery. This leads to much higher heat generation rates and higher temperatures in the neighborhood of the tabs, and the temperature decreases towards the lower half of the cell (positive dT/dy). During charge and discharge experiments, it was apparent that the heat generation is uniform in the x-direction but noticeably changes in the y-direction. Also note that thermistors are placed at each tab as shown in Fig. 2 to monitor its temperature as well.

2.2. Calibration of TLC strips

In order to obtain reliable and accurate temperature data from the TLC strips they must first be carefully calibrated. These strips are extremely sensitive and therefore all variables within the environment must be carefully controlled. Any changes in the illumination intensity, illumination angle, or orientation of the camera relative to the region of interest can affect the accuracy of the final data. Because the actual color reflected by the TLC depends both on the view angle, it is necessary to include the (x, y) coordinate of the TLC in the calibration process. As a result, the mapping between the TLC's color and its temperature is a function of the (x, y) coordinate of the TLC on the surface of the cell.

The calibration process consists of heating the TLC to a uniform temperature, and acquiring a color image. The process is repeated over the entire temperature range in 1-degree increments. Fig. 3 shows a solid model of the aluminum heater block used for TLC calibration. The black section in the center represents the five TLC strips. Three grooves were cut on the right side to accept thermistors. The thermistors were epoxied to inserts which were threaded directly into the aluminum block allowing accurate surface temperature measurement at three locations in the y-direction. The aluminum block is heated by a strip heater with a controller to regulate the amount of heat being generated. Strip heaters, however, do not generate heat evenly. Therefore, the strip heater was bonded to the back of a 50 mm thick aluminum block. The high thermal conductivity of aluminum allows the heat to diffuse evenly in the x–y direction and present an isothermal condition for the TLC. The temperature readings of the three thermistors were closely monitored during calibration to ensure isothermal conditions.

The calibration is conducted by slowly increasing the amount of heat generated by the strip heater. When each of the three thermistors reads to within ±0.2 °C of an integer value between 25 and 50 °C, an image is acquired. These images are stored for subsequent processing using a Matlab code. Each TLC strip is divided into 26 regions vertically (see Fig. 4) to account for the y-variation in illumination and view angle. In addition, since each of the five TLC strips is calibrated separately, the sensitivity in the x-direction is also accounted for. Color data were recorded for each temperature value in the calibration process. Hue values are then generated from the color data. Hue values are especially useful for TLC thermography as they increase monotonically with temperature. Fig. 5 shows calibration data for the rightmost TLC strip.

A second Matlab code was written to convert TLC color images acquired during battery experiments into temperature values using the calibration data. The program first converts the color image into hue values for each of the 26 regions. Next, it compares the hue value for a given region with the hue values from the calibration data files, and calculates the corresponding temperature by interpolation for each region. In this way, temperature measurements are obtained from the entire surface of the cell covered by the TLC strips. A thermocouple fixed to the surface of the cell was used to ensure proper calibration of the TLC strips. It was confirmed that the TLC strips measured the temperature of the cell's surface to an accuracy of ±0.5 °C.

In addition to TLC image processing, a LABVIEW program was used to record thermistor data from each of the cell's terminals with respect to time.

2.3. Cooling system

Now that the surface temperature field of the entire cell could be accurately monitored, a cooling system was designed and installed.

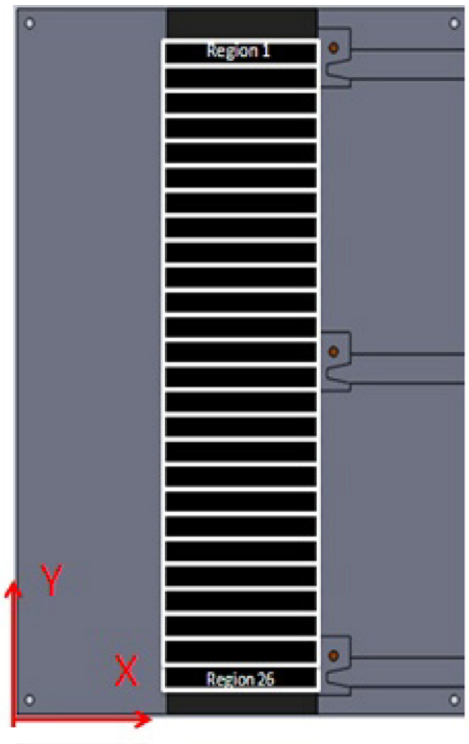

Fig. 4. TLC strips were divided into 26 regions to account for the *y*-variation in illumination and view angle. The sensitivity in the *x*-direction is also accounted for as each of the five strips is calibrated separately.

The design consisted of 4.76 mm thick aluminum cooling plates inserted between adjacent cells. The in-plane dimensions of the aluminum plate were identical to those of the cell. A 6.35 mm ID aluminum pipe was welded to the top edge of each cooling plate. The entire stack comprising five cells and four cooling plates was compressed before testing to ensure good thermal contact between the cells and the plates. Manifolds were constructed for both inlet and outlet so that the coolant flow (water) was evenly distributed between each cooling channel. The inlet manifold was supplied by a chilled water line in the lab. Both the inlet flow temperature and flow rate were held constant during the experiments. Custom thermistor mounts were fabricated to monitor the inlet and outlet temperatures on one of the channels. This data was useful in calculating the total heat extracted from the cells. Fig. 6 shows the experimental layout.

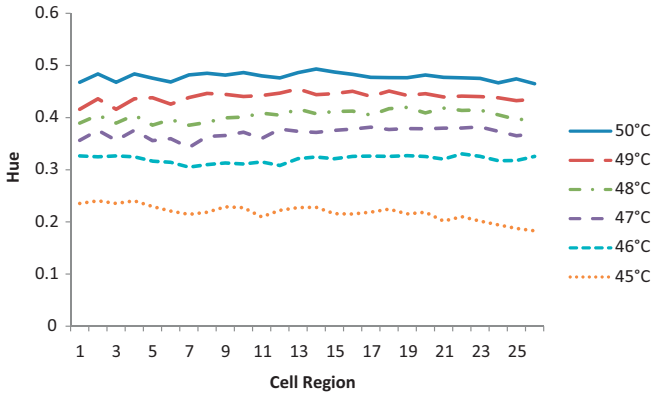

Fig. 5. Calibration data for the 45–50 °C TLC strip. The *x*-axis represents the 26 regions (top to bottom) of the TLC strip, and the *y*-axis is the hue value for each of those regions. The slight fluctuations in the data indicate that careful calibration is necessary for accurate results.

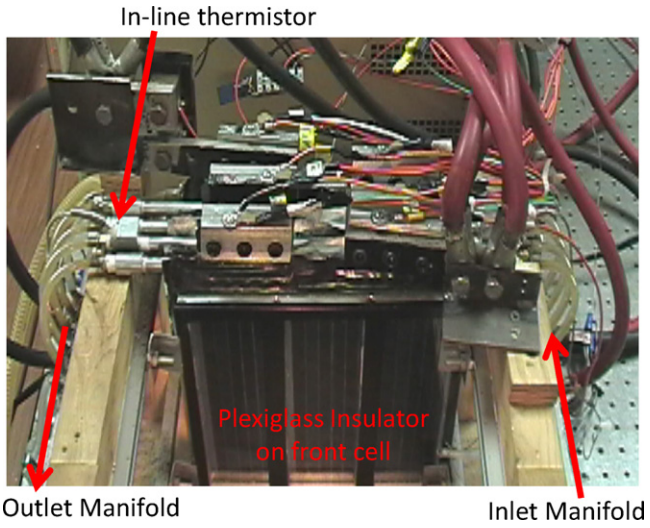

Fig. 6. Experimental layout of the cooling system for the stack of five cells. The inlet and outlet manifolds distribute water evenly between each of the four cooling channels while the thermistors provide water temperature readings.

In order to test these cells in the lab, a power source capable of supplying 400 A charging current was acquired. The cells were discharged through a bank of 24 0.6-Ω resistors wired in parallel. Each resistor was connected to a relay that could be switched on or off depending on how much current the user wants to draw. At full resistance it was possible to draw over 300 A of discharge current from the cells. The same LABVIEW program that recorded thermistor data was also used to regulate the current. This program allowed the user to activate the desired number of resistors for discharging, or to enter the current value for charging. The fuel cell hybrid bus in use on the University of Delaware campus [13] only demands charge and discharge currents up to 300 A. Hence, our experiments were held under this current limit.

2.4. Testing protocol

The first test was conducted at 300 A. The cells were subjected to 5-min charge and discharge cycles until the 50 °C threshold was reached, or 90 min had elapsed. The test was conducted first without activating the cooling system, and then repeated with a coolant water flow rate of 0.0315 kg s^{-1} per channel. The surface temperature variation of the cell was recorded by acquiring TLC images at 1-min increments for the duration of the trials. These images were stored for post-processing with the Matlab code. The TLC data along with the thermistor data provided temperature versus time curves that were used to quantify the effectiveness of the cooling system. The same tests were repeated at 200 A, and at 100 A since these belong in the range of currents experienced by the cells under normal operating conditions. At these lower current levels the tests were only conducted for 60 min as a steady state was reached more rapidly.

A second set of tests was conducted to determine the total heat generation in each cell during charge and discharge cycles by measuring the temperature rise of the coolant as it flowed through the stack. The previous tests employed a high flow rate of water that resulted in a temperature rise that was too small to be accurately resolved by the thermistors. Hence, the flow rate was decreased to 0.0063 kg s^{-1} per channel in the second set of tests. These tests used the same charge cycles and currents as the previous set of three tests.

Safety is of utmost importance when working with such large currents. During testing, the portion of the room containing the

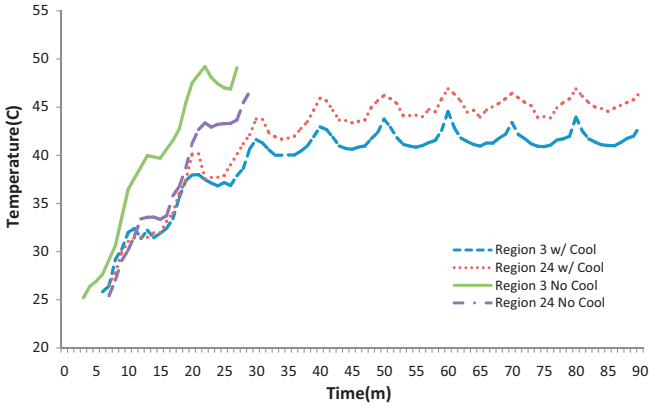

Fig. 7. Temperature versus time for the 300 A test with and without cooling. Maximum temperatures are reached very quickly without cooling, proving the need for an active cooling system. At a coolant flow rate of 0.0315 kg s^{-1} steady state is reached around 45 °C.

experimental setup was isolated to prevent accidental entry by lab personnel and eliminate the potential for injury.

3. Results and discussion

Each curve on the following temperature versus time graphs represents the temperature at specific locations on the cell. Region 3 is at the top of the cell near the terminals and region 24 is close to the bottom. Tab 5 is the thermistor data from the positive interconnect on the front cell.

3.1. 300 A charge and discharge cycling

Fig. 7 presents temperature data for the 300 A test with and without cooling. This plot clearly demonstrates the need for a cooling system as the temperature rises rapidly in the absence of cooling. In fact, the test without cooling had to be terminated at 30 min to prevent cell damage because the threshold temperature of 50 °C had already been reached. Also note that the top of the cell (Region 3) is always hotter than the bottom (Region 24). This is due to the higher heat generation at the top of the cell as well as the heat generated due to contact resistance at each terminal's connection.

The temperature profiles are dramatically different when the cooling system is in operation at 0.0315 kg s^{-1} of water flow per channel. Fig. 7 shows that the threshold temperature of 50 °C is not reached even after 90 min of testing. The temperature plots indicate that the system has reached a steady state around 45 °C, something that was not observed in the absence of cooling. It is also important to realize that the two curves from the top (Region 3) and bottom (Region 24) of the cell present virtually the same temperature versus time profile up to about the 14-min mark with cooling. This implies that the higher heat generation in Region 3 is countered by a more effective heat removal due to its proximity to the cooling channel. Beyond 14 min, the two curves diverge and maintain about a 5° difference at steady state. It is also interesting to note that the top of the cell is now cooler than the bottom. This proves that the cooling system design is quite effective in removing heat from the region where it is most intensely generated.

Another interesting phenomenon seen in Fig. 7 is the periodic fluctuations in the temperature profiles. These fluctuations are more evident in the curves with cooling, and are strongly correlated with the periodicity of the charge and discharge cycles. Discharge cycles generate more heat due to the entropy term as explained below. The heat generated in the cell can is expressed as:

$$q = I^2R - IT\frac{dV_{oc}}{dT} \quad (2)$$

where q is the heat generated, I is the current, R is the resistance, T is the absolute temperature, and V_{oc} is the open circuit voltage of the cell. The first term on the right side of the equation refers to the heating due to ohmic resistance. The second term is the entropy term. Discharge currents occur when $I > 0$, whereas the term dV_{oc}/dT is always negative. Consequently, the second term on the right hand side is positive during discharge and negative during charge. The change in sign of the second term during charge/discharge cycling accounts for the periodicity in heat generation, and hence the wavy appearance of the temperature versus time profiles in Fig. 7.

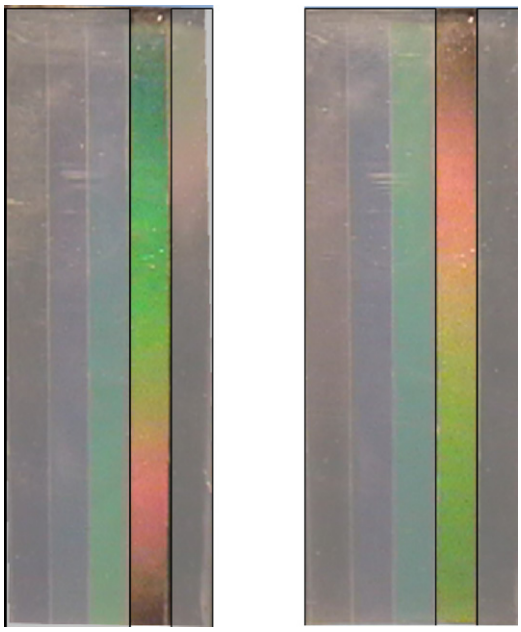

Fig. 8. Left: temperature visualization 18 min into the 300 A test without cooling. Right: the same Image 34 min into the test with cooling. The activation of the cooling system causes the temperature profile to invert.

The effect of the cooling system can be visually inferred by examining Fig. 8. The image on the left shows the temperature distribution at 18 min into the test without cooling, while the image on the right is at 34 min into the test with cooling. It is seen that the fourth strip from the left is the active strip, indicating that the cell temperature is in the 40–45 °C range in both views. As stated earlier, the red end of the color spectrum corresponds to cooler temperatures whereas the green and blue shades represent the warmer temperatures in the range. These images provide visual confirmation of the data in Fig. 7. The image at the left indicates that the upper half of the cell is warmer than the lower half. Conversely, the image on the right indicates that the upper half of the cell is cooler than the lower half. The two temperature distributions are almost exact inverses of one another demonstrating the impact of cooling, and the ability of the cooling system to remove heat from the cell.

3.2. 200 A charge and discharge cycling

The next test was run at 200 A with the same coolant flow rate of 0.0315 kg s^{-1}. Fig. 9 depicts the temperature data both with and without cooling for 5-min charge and discharge cycles at 200 A. In the absence of cooling, the cell temperature climbed continuously and approached the threshold temperature of 50 °C at about 60 min. It is also clear that the tab temperature remains hotter than the

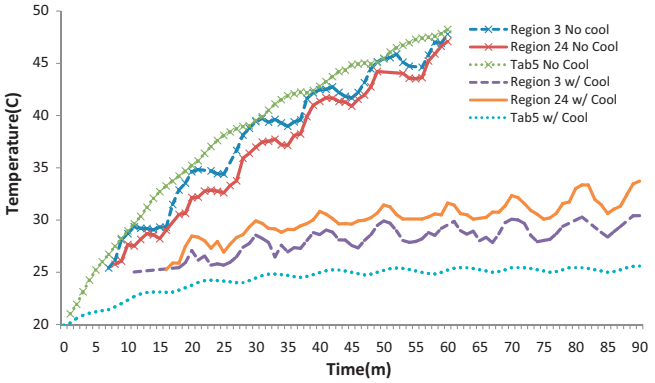

Fig. 9. Temperature versus time for the 200 A test with and without cooling. The threshold temperature of 50 °C is reached in 60 min with no cooling, indicating the need for a cooling system even at 200 A. With the cooling system in operation at 0.0315 kg s^{-1} a steady state is reached below 35 °C.

surface temperature of the cell at all times without active cooling. All three temperature traces show a continuously increasing trend even at the end of the testing period, implying that a steady state has not been reached. This indicates that an active cooling system is necessary even when cycling at a lower current value of 200 A. Also note that the top of the cell (Tab 5 and Region 3) is always hotter than the bottom (Region 24).

When the cooling system is activated the temperature profiles reach a steady state at less than 35 °C. As for the 300 A case, we can see that the lower half of the cell (Region 24) is warmer than the upper half (Region 3), while Tab 5 is the coolest point. Although the temperature at the bottom of the cell still increases during discharge, the cooling system is able to completely absorb nearly all of that heat when the cell is charging. The temperature of the tab appears to be trending towards a steady state at under 28 °C. With all parts of the cell approaching a steady state well under 55 °C, it is clear that this particular cooling system is effectively managing the heat generated by the cell at 200 A.

It is interesting to note in Fig. 9 that the tab temperature profile does not show a pronounced wavy appearance unlike the profiles for Regions 3 and 24. This is because the tab temperature is dominated by its local heat generation, which is purely due to contact resistance and therefore independent of the direction of current flow.

Fig. 10 shows the temperature distribution from the second TLC strip (30–35 °C) with and without cooling at 200 A. The image on the left is at 16 min without cooling, and the image on the right is at 47 min with cooling. Comparing these with the images from Fig. 8 shows the difference between 300 and 200 A battery cycles. The images on the right were taken within 2 min of each other into the test but they are very different. At 200 A the active thermochromic strip is 30–35 °C while at 300 A the active strip is 40–45 °C. Also, the temperature gradient is stronger at 300 A in the absence of cooling. Fig. 10 (left) shows mid-range yellow and green shades at the top (32–33 °C), but no indication of blue. In contrast, see Fig. 8, the top of the cell is nearly at the blue limit of the strip, nearing 45 °C.

3.3. 100 A charge and discharge cycling

The next test was run at 100 A (Fig. 11). At such a low current much less heat is generated. Even after 1 h of 100 A charge and discharge cycles in the absence of cooling, the temperature only climbs to 32 °C. However, it is possible that the temperature may exceed the 50 °C threshold in a longer test. With the cooling system operating at 0.0315 kg s^{-1} per channel the color play on the TLC strips was never activated, indicating that no

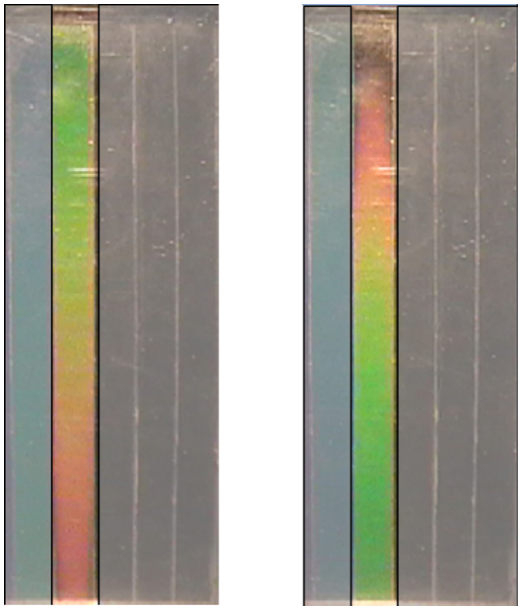

Fig. 10. Left: temperature visualization 16 min into the 200 A test without cooling. Right: the same Image 47 min into the test with cooling. As with the 300 A test, the cooling system effectively removes heat from the top of the cell where it is most intensely generated.

region on the cell ever exceeded 25 °C. Moreover, the thermistor on the cell's positive terminal (Tab 5) clearly shows a steady state temperature of about 19 °C which is well under the threshold temperature.

It is also important to note the temperature distribution in the cell (Fig. 12). Both panels in Fig. 12 show TLC images without cooling at 11 min (left), and 54 min (right) into the 100 A test. At the beginning of the test the top is hotter than the bottom resulting is a slight, positive, vertical temperature gradient. As time elapses the heat is able to distribute itself evenly throughout the cell, creating a more uniform temperature profile as shown in Fig. 12. Such an even distribution is possible because the cell does not generate as much heat at 100 A as it does at higher currents. The slight differences in temperature profiles of Regions 3 and 24 in Fig. 11 at later times can be attributed to the margin of error of the TLC temperature measurement.

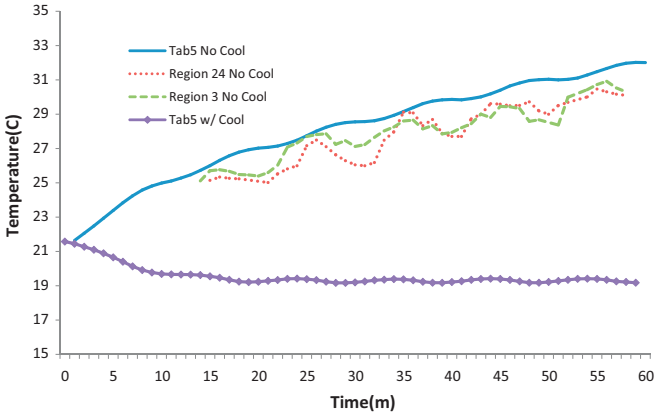

Fig. 11. Temperature versus time for the 100 A test with and without cooling. At such a low current, the threshold temperature is not approached even after 1 h of operation. However, there is no indication of steady state without cooling and the temperature may eventually exceed 50 °C. With a coolant flow of 0.0315 kg s^{-1}, Tab 5 reaches a steady state below 20 °C, and the TLC strips are never activated.

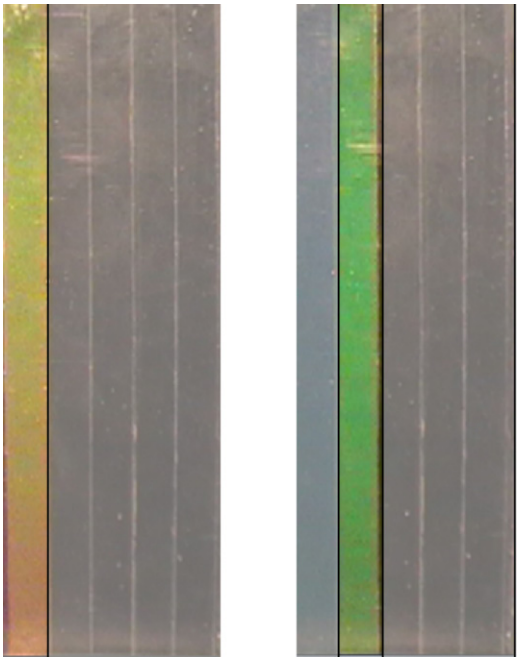

Fig. 12. Left: temperature visualization 11 min into the 100 A test without cooling. Right: 54 min into the same test also without cooling. Note that there is a slight (positive) temperature gradient at 11 min but by the end of the test the temperature profile appears to be nearly uniform. Lower currents cause a smaller heat generation and therefore more even temperature distribution.

3.4. Total heat flux measurements

For the next set of tests the coolant flow rate was reduced to 0.0063 kg s^{-1} per channel to increase the temperature rise of the coolant from inlet to exit. As a result, the change in coolant temperature could be adequately resolved by the thermistors whose least count is ±0.2 °C.

The heat extracted by the coolant is given by:

$$Q_{channel} = \dot{m} C_p (T_{outlet} - T_{inlet}) \quad (3)$$

where $Q_{channel}$ is the heat extracted by the cooling channel, $\dot{m}$ is the coolant mass flux, and C_p is the specific heat of water. At steady state, the heat balance for the cell can be expressed as:

$$Q_{cell} = Q_{NC} + Q_{channel} - Q_{tabs} \quad (4)$$

where Q_{cell} is the heat generated by each cell, C_p is the heat lost due to natural convection from its exposed surfaces, and Q_{tabs} is the heat generated due to contact resistance at the tabs. Note that Eq. (4) is only valid at steady state because the amount of heat stored in the aluminum plates and the cell itself has not been included in the analysis. The heat generated in the tabs is estimated as:

$$Q_{tabs} = I^2 R \quad (5)$$

To find the contact resistance, a current was run through the cells and the voltage drop was measured across the tabs:

$$R = \frac{V}{I} \quad (6)$$

The average contact resistance was computed as 2.4E−5Ω. To find the heat lost by natural convection we use:

$$Q_{NC} = Ah(T_{cell} - T_{ambient}) \quad (7)$$

where A is the exposed surface area, and h is the heat transfer coefficient.

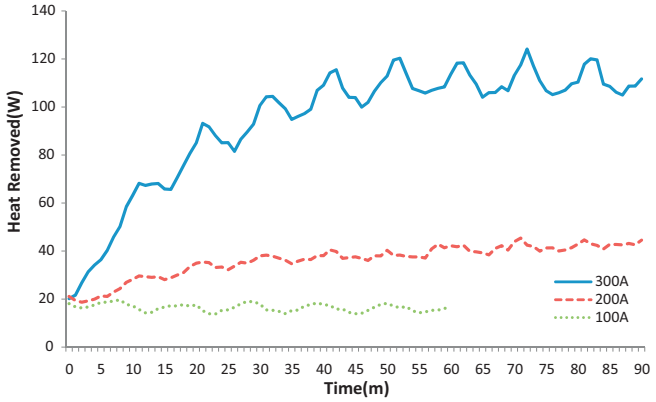

Fig. 13. Heat removed versus time for 100, 200 and 300 A cycles. These curves approach steady state in a manner similar to the temperature versus time graphs.

Table 1
Values of heat generation and removal rates computed from Eqs. (3)–(7) for the three current demands at steady state.

	$Q_{channel}$ (W)	Q_{NC} (W)	Q_{tabs} (W)	Q_{cell} (W)
100 A	16.1	0	0.2	15.9
200 A	38	2.5	1	39.5
300 A	94.8	4.3	2.2	92.6

The energy balance was performed by running the same charge and discharge cycles as before at 100, 200, and 300 A. The data in Fig. 13 were generated from Eq. (3).

The heat generated by the cell during 300, 200 and 100 A charge cycles is determined following the procedure outlined in Eqs (4)–(7). Note again that this analysis is only valid at steady state. Table 1 lists the steady-state values of $Q_{channel}$, Q_{NC}, Q_{tabs}, and Q_{cell} for the three current values tested.

For 300 A the time period from 40 to 45 min is examined because the cell is in a charge cycle and the temperature remains nearly constant. At 200 A the average heat removed from 50 to 55 min is used for the same reason. For 100 A charge cycles, the heat lost to natural convection can be ignored because the cell temperature never exceeds room temperature. These data were examined in the 30–35 min time period. As expected, Table 1 indicates that the heat generation rate within the cell increases with the charge/discharge current to a maximum value of 92.6 W at 300 A. Yet, the cooling system developed here is able to restrict the cell temperature to within the desired limit.

4. Conclusions

By developing a method to determine the entire surface temperature field of a lithium–titanate cell we were able to draw important conclusions and develop a path forward for further research. First, these cells do not generate heat evenly throughout their volume. Instead, a higher amount of heat is generated in the region of the cell close to the terminals. Thermochromic liquid crystal thermography clearly revealed the temperature gradients across the face of the cell. Battery temperature measurements were conducted at 100, 200, and 300 A charge/discharge cycles. At 300 A, the cell temperature rises very rapidly proving that an active cooling system is definitely required. At 200 A, although the temperature rise is slower, an active cooling system is still required. At 100 A, the heating rate is small enough that active cooling may not be required. The actual heat generated by the cell during each of these current cycles was also experimentally measured as 16, 50 and 93 W at 100, 200 and 300 A, respectively. Using the experimentally determined temperature distribution and boundary conditions, it is possible

to write an algorithm to extract the heat generation term as a function of the in-plane spatial coordinate of the cell. An accurate heat generation term is essential in developing a complete thermal model of the cell. The value of such models is that various cooling system designs can be tested in computer simulations prior to fabrication.

We also determined that the liquid-cooled system is a viable option for the thermal management of the cells. During the 300 A test the cooling system was able to restrict the steady state cell temperature to below 50 °C. In actual driving conditions the current demand is rarely this high. The cells will most often be functioning in the 100–200 A range. Our cooling system was easily able to cool the batteries at these currents and approach a steady state well below the maximum operating temperature. Liquid cooling, however, may not be the best option as it requires a chiller to cool the liquid and a pump to circulate it through all of the cooling channels. With EVs carrying hundreds of cells, the parasitic power required to drive such a system would be substantial. Hence, our future goal is to seek a system that can effectively manage the temperature of the cells while exhibiting the least parasitic losses.

Acknowledgements

This work was funded by a grant from the Federal Transit Administration. We are grateful to Doug Brunner, Adam Kinzey and Piyush Bubna for their help with this research.

References

[1] A. Gotcher, Nanostructered electrodes: experts have recognized for year the advantages of lithium ion technology over traditional power batteries, particularly those based on lead acid chemistry, Adv. Mater. Process. 163 (12) (2005) 32–38.
[2] J. Melendez, A. Foronda, J.M. Aranda, F. Lopez, F.J. Lopez del Cerro, Infrared thermography of solid surfaces in a fire, Meas. Sci. Technol. 21 (2010) 105504–105514.
[3] K. Yang, J.J. An, S. Chen, Temperature characterization analysis of $LiFePO_4$/C power battery during charging and discharging, J. Therm. Anal. Calorim. 99 (2010) 515–521.
[4] D. Dabiri, Digital particle image thermometry/velocimetry: a review, Exp. Fluids 46 (2008) 191–241.
[5] N. Abdullah, A.R.A. Talib, A.A. Jaafar, M.A.M. Salleh, The basics and issues of thermochromic liquid crystal calibrations, Exp. Therm. Fluid Sci. 34 (2010) 1089–1121.
[6] Y. Rao, S. Zang, Calibrations and the measurement uncertainty of wide band liquid crystal thermography, Meas. Sci. Technol. 21 (2010) 015105–015113.
[7] K.H. Kwon, C.B. Shin, T.H. Kang, C. Kim, A two-dimensional modeling of a lithium polymer battery, J. Power Sources 163 (2006) 151–157.
[8] L. Cai, R.E. White, An efficient electrochemical-thermal model for a lithium-ion cell by using the proper orthogonal decomposition method, J. Electrochem. Soc. 157 (2010) A1188–A1195.
[9] L. DaHe, Y. Kai, C. Shei, W. Feng, Thermal behavior simulation of Ni/MH battery, Chin. Sci. Bull. 54 (9) (2009) 1500–1506.
[10] M. Sievers, U. Sievers, S.S. Mao, Thermal modeling of new Li-ion cell design modifications, Forsch Ingenieurwes 74 (2010) 215–231.
[11] S.C. Chen, C.C. Wan, Y.Y. Wang, Thermal analysis of lithium-ion batteries, J. Power Sources 140 (2005) 111–124.
[12] U.S. Kim, C.B. Shin, C. Kim, Modeling for the scale-up of a lithium-ion polymer battery, J. Power Sources 189 (2009) 841–846.
[13] P. Bubna, D. Brunner, J.J. Gangloff, S.G. Advani, A.K. Prasad, Analysis, operation and maintenance of a fuel cell/battery series-hybrid bus for urban transit applications, J. Power Sources 195 (2010) 3939–3949.